Charge Localization in Cs<inf>2</inf>AgBiBr<inf>6</inf> Double Perovskite: Small Polarons and Self-Trapped Excitons

THE JOURNAL OF PHYSICAL CHEMISTRY C
A JOURNAL OF THE AMERICAN CHEMICAL SOCIETY

pubs.acs.org/JPCC
Article

Charge Localization in $Cs_2AgBiBr_6$ Double Perovskite: Small Polarons and Self-Trapped Excitons

Mehmet Baskurt and Julia Wiktor*

Cite This: J. Phys. Chem. C 2023, 127, 23966−23972
Read Online

ABSTRACT: Halide double perovskites have gained significant interest as promising materials in optoelectronic applications. Their relatively soft structure allows deformations that can potentially trap charge carriers, leading to the formation of small polarons. In this study, we investigate hole and electron polarons in $Cs_2AgBiBr_6$, a promising double perovskite, using the PBE0(α) functional. Our results reveal that spin−orbit coupling has a significant effect on the formation energies of small polarons and must be considered for accurate modeling of localized charges in $Cs_2AgBiBr_6$. While electron localization on Bi atoms is favorable, the hole polaron localized at the Ag site is very close in energy to the delocalized state. Simultaneous localization of holes and electrons at neighboring Ag and Bi sites leads to the formation of self-trapped excitons due to the significant attraction between the polarons of opposite charges. Our results provide insights into the essential properties of $Cs_2AgBiBr_6$ and have potential implications for further research and development of $Cs_2AgBiBr_6$-based green devices.

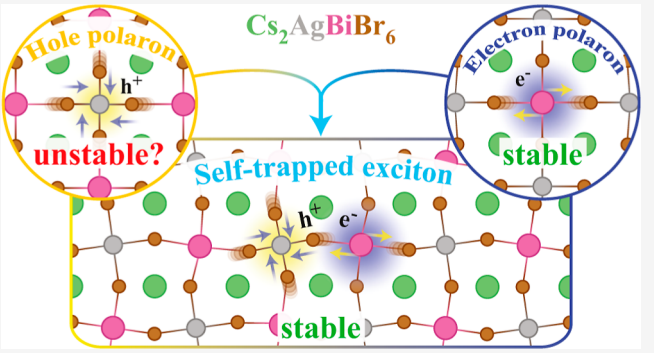

INTRODUCTION

Halide perovskites have attracted significant attention in the scientific community in recent years due to their exceptional optoelectronic properties.[1,2] In particular, their high power conversion efficiencies have led to their use in the design of high-efficiency solar cells, with efficiencies surpassing 25%.[3] Additionally, halide perovskites have been explored for use in a variety of other technologies, such as light-emitting diodes,[4,5] lasers,[6] memories,[7] transistors,[8] batteries,[9] X-ray detectors,[10] and gas sensors.[11] However, the most efficient halide perovskites contain lead, which exhibits high toxicity. One possibility to eliminate this issue is to use halide double perovskites, such as $Cs_2AgBiBr_6$,[12−15] where the metal cation in the +2 oxidation state is replaced by the combination of cations in +1 and +3 states.

The nature of excess charges and their mobility are two of the most important factors determining the performance of materials used in optoelectronic devices. Understanding these properties is crucial for the development of new materials with improved performance. Recent experimental works[16−19] reported that excess charges in $Cs_2AgBiBr_6$ are subject to self-trapping[16] and in particular showed that the charge carriers in this material undergo an ultrafast, barrier-free self-localization process from an initially mobile delocalized state to a self-trapped, small polaronic state, which diffuses to an emitting color center, revealing an important mechanism for the charge transport and emission properties of the material. This strong trapping is in contrast to the situation in the more studied single-halide perovskites, such as methylammonium lead iodide (MAPI), where a larger extent of charge localization has been proposed.[20−23] While there is a clear need to investigate charge trapping in double perovskites more closely, theoretical investigations on small polarons in this class of materials are lacking. In the present work, we focus on $Cs_2AgBiBr_6$ as a representative case of the larger family of double-halide perovskites and computationally assess the nature of self-trapping in these materials.

From a computational point of view, simulation of small polarons poses a challenge since it requires overcoming the self-interaction error related to the use of standard density functional theory (DFT).[24,25] To remove the aforementioned error, we use the hybrid functional PBE0(α), satisfying the generalized Koopmans' theorem,[26−28] where α is fraction of the Fock exchange. Hybrid functionals based on the Koopmans' conditions have been shown to well describe the polaronic distortions and to give band gaps with high accuracy without resorting to computationally more demanding *GW* calculations.[29] An additional challenge in computational

Received: October 2, 2023
Revised: November 10, 2023
Accepted: November 13, 2023
Published: November 30, 2023

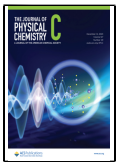

https://doi.org/10.1021/acs.jpcc.3c06551
J. Phys. Chem. C 2023, 127, 23966−23972

studies on halide perovskites is related to strong local disorder in the cubic phase of these materials.[30−33] It has been shown that the perfect cubic structure at 0 K does not represent well the dynamical structure at finite temperatures, which is only cubic on average. One of the ways of overcoming this issue is through the use of the so-called "polymorphous" models proposed by Zhao et al. in ref 31. In the present work, we perform calculations in both monomorphous (perfect cubic) and polymorphous (disordered) structures of $Cs_2AgBiBr_6$ to assess the effect of local disorder on polaron formation. Our calculations indicate that charge localization is slightly more favorable in the polymorphous structure. We also examine the effects of spin−orbit coupling (SOC) interactions on the formation energies of the polarons and find that SOC significantly stabilizes the electron polaron. With these two effects considered, the formation of electron polarons in the $Cs_2AgBiBr_6$ lattice is favorable, while the hole polarons are marginally unstable. Finally, we determine the formation of the self-trapped exciton (STE) by examining the interaction between the neighboring hole and the electron polarons. The information gained from this study provides insight into the essential properties of $Cs_2AgBiBr_6$, and we anticipate that it will have important implications for future applications in sustainable optoelectronic devices.

METHODS

In the present study, we use two DFT packages, CP2K[34,35] to perform fast search and assessment of possible polaronic configurations and the Vienna ab initio simulation package (VASP)[36,37] to achieve more accurate estimates of polaronic formation energies, including SOC.

Within CP2K, Goedecker−Teter−Hutter pseudopotentials are employed to describe the core−valence interactions[38] together with the DZVP-MOLOPT basis sets.[39] We set the cutoff energy for the plane-wave basis set to 400 Ry. The PBE0(α)[40] functional with the auxiliary density matrix method[41] is used to perform calculations at the hybrid functional level. We use CP2K to find and explore possible polaronic configurations.

Since the hybrid functional calculations in the CP2K package do not allow for the inclusion of the SOC effect and underestimate the band gap of $Cs_2AgBiBr_6$ in the current computational setting (see discussion in Supporting Information), final calculations are performed using VASP.[36,37] Within VASP, we run single-shot simulations on top of optimized structures taken from CP2K. We use the plane-wave projector-augmented wave method with the following valence configurations: Cs [5s5p6s], Ag [5s4d], Bi [6s6p], and Br [4s4p].[42] The plane-wave cutoff energy is set to 300 eV, and the convergence criterion between consequent steps is set to 10^{-4} eV. Calculations are run at the PBE0(α) level of theory, and the Brillouin zone is sampled at the Γ point.

To assess the stability of various polaronic states, we calculate the corresponding formation energies with respect to a pristine unit cell containing a delocalized excess charge, represented by the energy of conduction band minimum (CBM) or valence band maximum (VBM). The polaron formation energy, E_f, is calculated as

$$E_f = E_{polaron} - E_{pristine} + q\epsilon_{CBM,VBM} + E_{corr} \quad (1)$$

where $E_{polaron}$ is the total energy of the charged cell with polaron, $E_{pristine}$ is the total energy of the neutral pristine cell, q is the extra charge in the system (+1 for hole, −1 for electron), $\epsilon_{CBM,\ VBM}$ is the energy of the relevant delocalized state (for q = −1, CBM; q = +1, VBM), and E_{corr} is the finite-size correction term that is calculated based on the scheme proposed by Freysoldt, Neugebauer, and Van de Walle.[43]

Polaron formation energy difference due to SOC effects, Δ^{SOC}, is calculated as

$$\Delta^{SOC} = E_f^{withSOC} - E_f^{w/oSOC} \quad (2)$$

where $E_f^{withSOC}$ is the polaron formation energy with SOC, and $E_f^{w/oSOC}$ is the polaron formation energy without SOC.

We also study the interaction between the hole and electron polarons to assess the possibility of the formation of STEs. Initially, we conduct calculations in a simulation cell that is in a triplet state without considering the effects of SOC. However, in the calculations with SOC, we cannot perform a triplet calculation in the same way as in the spin-polarized case. Therefore, we specify the occupied and unoccupied states that correspond to electron and hole states in the calculations without SOC. We note that the excited state is here described by a single Slater determinant, which in principle approximately represents the first singlet and triplet excited states.[44,45] In the case of the singlet state, the spin purification procedure is required to obtain an accurate prediction of its energetic, while the energy of the lowest triplet state is usually not corrected.[46] While we focus on the triplet state in this study, we note that an energy difference of about 80 meV was found between the triplet and singlet states, suggesting that the correction for the singlet energy is also of that order. The formation energy of STE, E_f^{STE}, where the self-trapped hole and electron are located in neighboring octahedra is calculated by

$$E_f^{STE} = E_{STE} - E_{pristine} + \epsilon_{VBM} - \epsilon_{CBM} \quad (3)$$

where $E_{exciton}$ is the total energy of the cell with STE and $E_{pristine}$ is the total energy of the neutral pristine structure. The binding energy of the STE, E_b^{STE}, is calculated as

$$E_b^{STE} = E_f^{STE} - E_f^{hole} - E_f^{electron} \quad (4)$$

where E_f^{hole} and $E_f^{electron}$ are the formation energies of the hole and electron polarons, respectively, as described in eq 1.

RESULTS AND DISCUSSION

We first determine α in the hybrid functional, for which the self-interaction error vanishes. This is done through enforcing the Koopmans' condition.[26,27] In the calculations, a 2 × 2 × 2 supercell of $Cs_2AgBiBr_6$ in the $Fm\bar{3}m$ phase consisting of 320 atoms is used. The optimal fraction α of Fock exchange in PBE(α) that satisfies Koopmans' theorem is determined by calculating the empty and occupied single-particle energy level of a single Br vacancy. In order to account for electrostatic interactions between periodic images of the charge, finite-size corrections are applied.[47] Literature values of high-frequency and static dielectric constants ϵ_∞ (5.42) and ϵ_0 (16.73) are used in the corrections.[48] Calculations are carried out for three different fractions, α = 0.40, α = 0.50, and α = 0.60. By choosing relatively high α values, we ensure that the defect charge is localized. Using the linear relation between fraction of Fock exchange and the single-particle energy levels that is reported by Miceli et al.,[29] we can determine the optimal α value by extrapolating the value for which the position of the occupied and unoccupied levels coincide. As shown in Figure 1, after applying finite-size corrections, the Fock exchange α is determined to be 0.30 in the CP2K package and 0.28 in the VASP

https://doi.org/10.1021/acs.jpcc.3c06551
J. Phys. Chem. C 2023, 127, 23966−23972

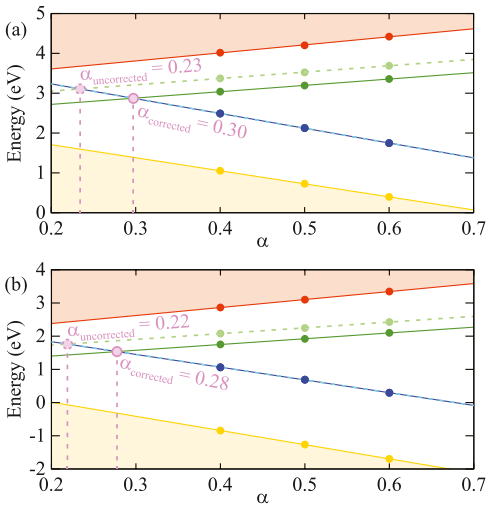

Figure 1. Band edges and single-particle energy levels of the Br vacancy with respect to the fraction of Fock exchange α used in PBE0(α) calculations, determined using (a) CP2K and (b) VASP. Dashed and solid lines represent values excluding and including the finite-size corrections, respectively. Blue and green correspond to the neutral and positive charge states of the defect.

package. We note that the uncorrected values of α are 0.23 and 0.22 for CP2K and VASP packages, respectively, highlighting the necessity of including finite-size correction in the procedure.[47,49,50] In the subsequent steps of our analysis, we optimized the structures using the CP2K package, with a Fock exchange alpha value set to α = 0.30. We then calculated the total energies of the optimized structures and analyzed the electronic states using the VASP package, with the α value of 0.28.

We note that the fundamental indirect band gap yielded by the PBE0 functional with α = 0.28 (including SOC) is 2.7 eV. This is higher than previously reported values of about 2.0 eV.[16,52] However, the extraction of the fundamental indirect band gap from the absorption spectra is rather complicated. Palummo et al.[53] identified indirect excitons in $Cs_2AgBiBr_6$, which would contribute to the absorption signal at about 2 eV. Therefore, this value does not necessarily need to correspond to the fundamental indirect band gap. Considering this complication, we can instead compare the fundamental direct band gap calculated within our hybrid functional (3.5 eV) with experiments. Wright et al.[16] estimated the fundamental direct band gap at low temperatures to be about 3.12 eV; however, the temperature dependence of the band gap exhibits some bending at low temperatures, implying significant effects of zero-point renormalization (ZPR). Linear extrapolation of the band gaps measured at higher temperatures in their study implies a 0 K-band gap without ZPR slightly above 3.2 eV. Kentsch et al.[54] reported a higher value at room temperature of 3.2 eV, which would imply a 0 K-band gap without ZPR of about 3.4 eV. Considering this range of values (3.2−3.4 eV), our fundamental direct band of 3.5 eV is in good agreement with experimental values, which validates the Koopmans functional used here.

Next, we focus on identifying polaronic distortions within the monomorphous model of $Cs_2AgBiBr_6$. Using a high initial alpha value (0.50) to facilitate charge localization, we distort

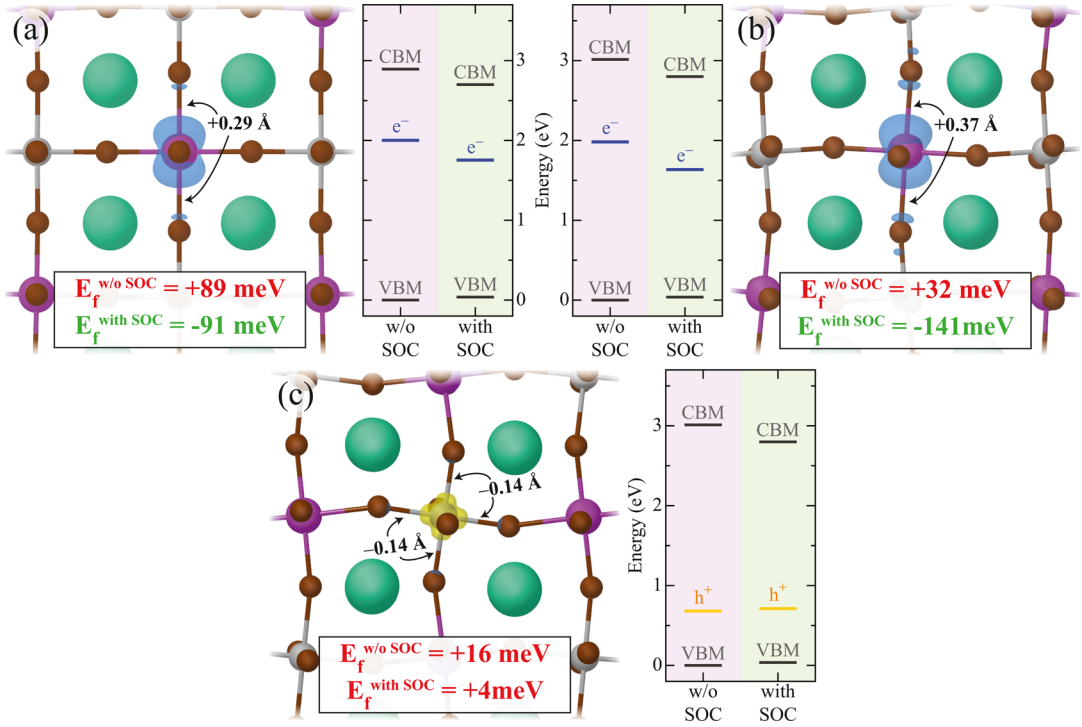

Figure 2. Band decomposed charge densities and energy level diagrams at Γ, without and with SOC effects for (a) electron polaron in the monomorphous cell, (b) electron polaron in the polymorphous cell, and (c) hole polaron in the polymorphous cell. In the insets, polaron formation energies including and ignoring SOC are given. Isosurface levels are displayed at 0.003 eV/Å^3, using VESTA software.[51] CBM and VBM levels are taken from the pristine cell. Polaron levels include finite-size corrections. Zero in the energy scale is set to the VBM of the pristine cell without SOC. Electron and hole polaron energy levels are indicated by blue and yellow colors. Arrows in the structures indicate the difference in the corresponding bond lengths.

https://doi.org/10.1021/acs.jpcc.3c06551
J. Phys. Chem. C 2023, 127, 23966−23972

Table 1. Polaron Formation Energies, E_f, Energy Levels of VBM and CBM of the Neutral Cell, ϵ_{VBM} and ϵ_{CBM}, and Polaron Level, $\epsilon_{Polaron}$, Calculated in the Monomorphous and Polymorphous Cells of $Cs_2AgBiBr_6$[a]

		without SOC				with SOC				
structure	polaron	E_f (meV)	ϵ_{VBM} (eV)	$\epsilon_{polaron}$ (eV)	ϵ_{CBM} (eV)	E_f (meV)	ϵ_{VBM} (eV)	$\epsilon_{polaron}$ (eV)	ϵ_{CBM} (eV)	Δ^{SOC} (meV)
monomorphous	electron	+89	0.00	2.00	2.89	−91	0.04	1.75	2.70	−180
polymorphous	electron	+32	0.00	1.98	3.02	−141	0.04	1.64	2.80	−173
	hole	+16	0.00	0.68	3.02	+4	0.04	0.71	2.80	−12

[a]Change in the formation energy due to SOC is given by Δ^{SOC}. VBM of the pristine cell where SOC effects are not considered is set to 0.

the Ag−Br and Bi−Br bonds and add, respectively, one excess hole or electron to each system in order to determine possible polaron configurations. The excess hole localizes on the Ag atom, contracting four Ag−Br bonds. The excess electron localizes on the Bi atom, leading to an increase in the length of two Bi−Br bonds. The polaronic geometries are shown in Figure 2.

With the geometries obtained from the previous step, we investigate the formation of the self-trapped hole and electron using the reduced Fock exchange alpha value that satisfies the Koopmans' condition (α = 0.30). Following structural optimization, the hole is found to be delocalized, whereas the electron remains localized on the Bi atom in the monomorphous cubic structure. Without SOC, the formation energy of the electron polaron is +89 meV, and the polaronic level is located at 892 meV below the CBM.

We now focus on the polymorphous model of $Cs_2AgBiBr_6$, since it has been reported that local distortions can significantly affect the electronic structure of cubic halide perovskites[31,55] We first generate several polymorphous structures and compare their energies with those of the monomorphous structure. The details on the structure generation along with energies of different structures are given in Supporting Information. As expected, all polymorphous cells are more stable than the monomorphous one. As a result, to obtain a more accurate description of the energetics of polaronic states in $Cs_2AgBiBr_6$, we carried out our calculations in the polymorphous structure.

We proceeded to investigate the small electron polaron in polymorphous $Cs_2AgBiBr_6$. Similar to the procedure adapted in the monomorphous cell, we add an excess electron to the structure, elongate the Bi−Br bonds surrounding a single Bi atom, and relax the structure with a high initial value of α (0.50), which is then reduced to 0.30. After relaxation, the electron remains localized on the Bi atom. The energy and electronic states of the system are then calculated, and the corresponding charge densities and energy levels are shown in Figure 2b. The formation energy of the electron polaron is determined to be +32 meV without SOC, and the polaron level is found to be located at 1.033 eV below the CBM in the polymorphous cell. Although the formation of the electron polaron remains energetically unfavorable, the polaron is observed to be more stable by 57 meV compared to the electron polaron in the monomorphous cell.

We then investigated the localization of the excess hole in the polymorphous cell. To achieve this, the Ag−Br bond lengths around a single Ag atom in the cell are decreased. The resulting structure is optimized first using α = 0.50, which is then decreased to 0.30. Unlike that in the monomorphous cell, the hole polaron remains localized after the final relaxation. At the same time, we observe that the charge localization induces not only the contraction of Ag−Br bonds but also a noticeable tilting of the whole $AgBr_6$ unit by 4.5° in comparison to the pristine polymorphous structure (see Figure 2c). We note that to achieve the same polaronic geometry in the monomorphous cell, the $AgBr_6$ unit would have to tilt by 10.1° compared to the initial state. We therefore conclude that the reason for a more favorable hole localization in the polymorphous cell is the facilitated octahedral tilting in this structure. The corresponding polaron level is located at 0.678 eV. The formation energy of the hole polaron is determined to be +16 meV, indicating that hole localization is not energetically favorable.

The calculations performed thus far have not included SOC effects. However, halide perovskites are known to be strongly influenced by relativistic effects, particularly at the CBM.[30,49,56] Hence, it is crucial to consider the influence of SOC on the polaronic states. Therefore, we calculate the effects of SOC on electron polaron in monomorphous and polymorphous cells and hole polaron in polymorphous cells. The results are shown in Figure 2. We observe that the stability of the polarons increases with the inclusion of SOC in $Cs_2AgBiBr_6$. This is in contrast to the situation in lead and tin halide perovskites, where SOC makes polaronic states less favorable.[49,57] While in the case of the hole polaron, the effect of SOC is weak (12 meV), the formation energy of the electron polaron is strongly reduced (by up to 180 meV). This strong stabilization is related to SOC making the single-particle level of the electron polaron lie deeper in the band gap relative to the CBM (see Table 1 for numerical values). The formation energy of the electron polaron, including SOC, is found to be −91 meV in the monomorphous structure and −141 meV in the polymorphous one. The stability of the electron polaron is in agreement with the experimental reports of barrier-free charge carrier localization in $Cs_2AgBiBr_6$.[16]

The hole polaron in the polymorphous structure is found to be marginally unstable, as evidenced by its positive formation energy of +4 meV. However, we note that this formation energy is below the expected accuracy of our computational setup, and we cannot rule out the possibility of the formation of hole polarons in $Cs_2AgBiBr_6$. Additionally, we found that the hole polaron is stabilized by facilitated octahedral tilting in the polymorphous cell. Therefore, it could also be stabilized by the thermal effect, which can lead to lattice softening and facilitate octahedral tilting.[49,58] Furthermore, we performed additional calculations at the equilibrium lattice constant, which gave a formation energy of −63 meV for the hole polaron (see Supporting Information). This suggests that the current computational setup is unable to rule out the hole localization.

Previous analyses focused on the localization of either holes or electrons separately. We now investigate the interaction between the opposite charges localized nearby. This is done by performing calculations in a cell with distorted neighboring $AgBr_6$ and $BiBr_6$ octahedra. After relaxation, we observe hole and electron localization on neighboring sites, as presented in Figure 3. We calculate the resulting formation energy of the STE according to eq 3 and find a value of −293 meV with

https://doi.org/10.1021/acs.jpcc.3c06551
J. Phys. Chem. C 2023, 127, 23966−23972

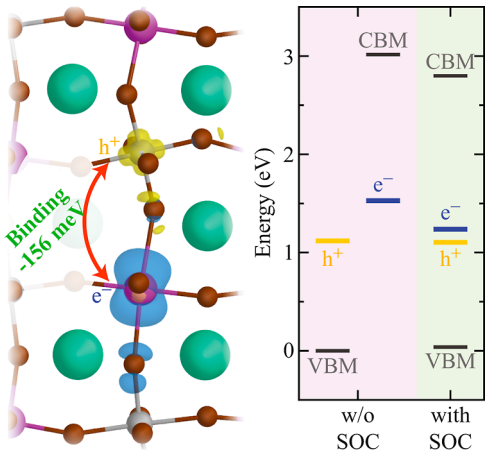

Figure 3. Isodensity of STE with the binding energy calculated including SOC, and the corresponding the energy diagram that shows VBM, CBM, electron (blue), and hole (yellow) levels. Zero in the energy scale is set to the VBM of the pristine cell without SOC. The isosurface level is taken as 0.0015 eV/Å^3.

SOC (−287 meV without SOC). This is significantly lower than the sum of the formation energies of separate hole and electron polarons (E_f^{hole} = +4 meV and $E_f^{electron}$ = −141 meV with SOC) within the corresponding computational setup. Therefore, we extract the binding energy E_b^{STE} = −156 meV (−335 meV without SOC) from the difference between these energies. Moreover, the electron−hole interaction also results in deeper single-particle states, which are now found at 1.56 eV (1.49 eV without SOC) below the CBM for the electron and 1.06 eV (1.12 eV without SOC) above the VBM for the hole.

We note that all results reported above have been obtained using the experimental lattice constant a = 11.27 Å.[59] To verify how our findings depend on this parameter, we also recalculated all formation energies at the equilibrium volume (a = 11.38 Å using PBE0(α) and including SOC). The results, reported in Supporting Information, differ by less than 0.1 eV from the ones calculated using the experimental lattice parameter and lead to the same general conclusions.

We now discuss our results in view of experimental studies on the behavior of excess charges in $Cs_2AgBiBr_6$. Photoluminescence (PL) measurements indicate that an essentially barrier-less self-trapping occurs in this material.[16] A PL signal has been detected at the energy of about 1.9 eV and assigned to a spatially localized color center.[60] The proposed self-trapping agrees well with the negative formation energy of the electron polaron and the STE found in this study. There are several possible energy transitions that could give rise to the observed PL signal. Initially, upon photoexcitation, an electron−hole pair, likely in the form of a free exciton, is generated. Subsequently, due to atomic relaxation, rapid formation of STEs could occur. Following the STE formation, the first conceivable transition would be the direct electron−hole recombination within the STE. It has been previously shown that this type of STE (related to a non-Jahn−Teller-like octahedral distortion) more likely leads to nonradiative transitions.[61] Another possibility would be the trapped electron recombining with a more delocalized hole from the valence band. The corresponding emission energy (based on differences between calculated single-particle levels) would be between 1.20 eV (electron from the STE) and 1.60 eV (electron polaron). This explanation is more plausible; however, the higher value of 1.60 eV is still significantly lower than the experimental value of 1.9 eV. The third option is the recombination of a hole trapped in the STE and a delocalized electron in the conduction band. This transition would correspond to 1.70 eV (see Table S5 in the Supporting Information), which is in better agreement with the experimental signal. We note, however, that the full understanding of photoluminescence from localized charges would require a more detailed study based on methods such as the Bethe-Salpeter equation or time-dependent DFT.[62,63]

CONCLUSIONS

In conclusion, we have studied charge trapping in $Cs_2AgBiBr_6$ by employing a Koopmans-compliant hybrid density functional. Possible modes of charge localization were identified by introducing excess holes and electrons and creating initial structural distortions. Excess holes were found to localize on Ag atoms, while excess electrons localized on Bi atoms. We compared charge localization in monomorphous and polymorphous models of $Cs_2AgBiBr_6$ and found that facilitated octahedral tilting leads to higher stability of hole polarons in the distorted model. The effects of SOC were also considered to provide a more accurate representation of the CBM and polaronic states. With SOC, electron localization was found to be energetically favorable in both monomorphous and polymorphous cells, with formation energies of −91 and −141 meV, respectively. On the other hand, hole polarons were found to be marginally unstable in the polymorphous structure at 0 K. Finally, the formation of STEs was assessed by considering holes and electrons localized at neighboring sites. We determined the binding energy of the STE to be −156 meV, including the SOC effect. Overall, our results reveal the intricate interplay between charge localization, the effects of SOC, and the stabilizing effect of neighboring electron and hole localization, forming STEs.

ASSOCIATED CONTENT

Supporting Information

The Supporting Information is available free of charge at https://pubs.acs.org/doi/10.1021/acs.jpcc.3c06551.

Generation and energy assessment of polymorphous structures, polaron formation energies and single-particle levels in optimal polymorphs, comparison between polaron energies and levels between CP2K and VASP, effect of the lattice parameter on polaron energies, and formation and binding energies of STE and corresponding energy levels (PDF)

AUTHOR INFORMATION

Corresponding Author

Julia Wiktor − *Department of Physics, Chalmers University of Technology, Gothenburg SE-412 96, Sweden;* orcid.org/0000-0003-3395-1104; Email: julia.wiktor@chalmers.se

Author

Mehmet Baskurt − *Department of Physics, Chalmers University of Technology, Gothenburg SE-412 96, Sweden;* orcid.org/0000-0001-7181-6814

Complete contact information is available at: https://pubs.acs.org/10.1021/acs.jpcc.3c06551

Notes

The authors declare no competing financial interest.

■ ACKNOWLEDGMENTS

The authors acknowledge funding from the "Area of Advance Materials Science" at Chalmers University of Technology, the Swedish Research Council (2019-03993), and the Swedish Strategic Research Foundation through a Future Research Leader programme (FFL21-0129). The computations were enabled by resources provided by the National Academic Infrastructure for Supercomputing in Sweden (NAISS) and the Swedish National Infrastructure for Computing (SNIC) at C3SE, NSC, and PDC.

■ REFERENCES

(1) Stranks, S. D.; Snaith, H. J. Metal-halide perovskites for photovoltaic and light-emitting devices. *Nat. Nanotechnol.* **2015**, *10*, 391−402.
(2) Dey, A.; Ye, J.; De, A.; Debroye, E.; Ha, S. K.; Bladt, E.; Kshirsagar, A. S.; Wang, Z.; Yin, J.; Wang, Y.; et al. State of the art and prospects for halide perovskite nanocrystals. *ACS Nano* **2021**, *15*, 10775−10981.
(3) Yoo, J. J.; Seo, G.; Chua, M. R.; Park, T. G.; Lu, Y.; Rotermund, F.; Kim, Y.-K.; Moon, C. S.; Jeon, N. J.; Correa-Baena, J.-P.; et al. Efficient perovskite solar cells via improved carrier management. *Nature* **2021**, *590*, 587−593.
(4) Lin, K.; Xing, J.; Quan, L. N.; de Arquer, F. P. G.; Gong, X.; Lu, J.; Xie, L.; Zhao, W.; Zhang, D.; Yan, C.; et al. Perovskite light-emitting diodes with external quantum efficiency exceeding 20 per cent. *Nature* **2018**, *562*, 245−248.
(5) Kim, Y.-H.; Kim, S.; Kakekhani, A.; Park, J.; Park, J.; Lee, Y.-H.; Xu, H.; Nagane, S.; Wexler, R. B.; Kim, D.-H.; et al. Comprehensive defect suppression in perovskite nanocrystals for high-efficiency light-emitting diodes. *Nat. Photonics* **2021**, *15*, 148−155.
(6) Shang, Q.; Li, M.; Zhao, L.; Chen, D.; Zhang, S.; Chen, S.; Gao, P.; Shen, C.; Xing, J.; Xing, G.; et al. Role of the exciton−polariton in a continuous-wave optically pumped $CsPbBr_3$ perovskite laser. *Nano Lett.* **2020**, *20*, 6636−6643.
(7) Gu, C.; Lee, J.-S. Flexible hybrid organic−inorganic perovskite memory. *ACS Nano* **2016**, *10*, 5413−5418.
(8) Yu, W.; Li, F.; Yu, L.; Niazi, M. R.; Zou, Y.; Corzo, D.; Basu, A.; Ma, C.; Dey, S.; Tietze, M. L.; et al. Single crystal hybrid perovskite field-effect transistors. *Nat. Commun.* **2018**, *9*, 5354.
(9) Ahmad, S.; George, C.; Beesley, D. J.; Baumberg, J. J.; De Volder, M. Photo-rechargeable organo-halide perovskite batteries. *Nano Lett.* **2018**, *18*, 1856−1862.
(10) Tsai, H.; Liu, F.; Shrestha, S.; Fernando, K.; Tretiak, S.; Scott, B.; Vo, D. T.; Strzalka, J.; Nie, W. A sensitive and robust thin-film x-ray detector using 2D layered perovskite diodes. *Sci. Adv.* **2020**, *6*, No. eaay0815.
(11) Shinde, P.; Patra, A.; Rout, C. S. A review on the sensing mechanisms and recent developments on metal halide-based perovskite gas sensors. *J. Mater. Chem. C* **2022**, *10*, 10196−10223.
(12) Chu, L.; Ahmad, W.; Liu, W.; Yang, J.; Zhang, R.; Sun, Y.; Yang, J.; Li, X. Lead-free halide double perovskite materials: a new superstar toward green and stable optoelectronic applications. *Nanomicro Lett.* **2019**, *11*, 16.
(13) Zhou, L.; Xu, Y.-F.; Chen, B.-X.; Kuang, D.-B.; Su, C.-Y. Synthesis and photocatalytic application of stable lead-free $Cs_2AgBiBr_6$ perovskite nanocrystals. *Small* **2018**, *14*, 1703762.
(14) Hoye, R. L. Z.; Eyre, L.; Wei, F.; Brivio, F.; Sadhanala, A.; Sun, S.; Li, W.; Zhang, K. H. L.; MacManus-Driscoll, J. L.; Bristowe, P. D.; et al. Fundamental carrier lifetime exceeding 1 μs in $Cs_2AgBiBr_6$ double perovskite. *Adv. Mater. Interfaces* **2018**, *5*, 1800464.
(15) Igbari, F.; Wang, R.; Wang, Z.-K.; Ma, X.-J.; Wang, Q.; Wang, K.-L.; Zhang, Y.; Liao, L.-S.; Yang, Y. Composition stoichiometry of $Cs_2AgBiBr_6$ films for highly efficient lead-free perovskite solar cells. *Nano Lett.* **2019**, *19*, 2066−2073.
(16) Wright, A. D.; Buizza, L. R.; Savill, K. J.; Longo, G.; Snaith, H. J.; Johnston, M. B.; Herz, L. M. Ultrafast excited-state localization in $Cs_2AgBiBr_6$ double perovskite. *J. Phys. Chem. Lett.* **2021**, *12*, 3352−3360.
(17) Caselli, V. M.; Thieme, J.; Jöbsis, H. J.; Phadke, S. A.; Zhao, J.; Hutter, E. M.; Savenije, T. J. Traps in the spotlight: How traps affect the charge carrier dynamics in $Cs_2AgBiBr_6$ perovskite. *Cell Rep. Phys. Sci.* **2022**, *3*, 101055.
(18) Tailor, N. K.; Parikh, N.; Yadav, P.; Satapathi, S. Dielectric Relaxation and Polaron Hopping in $Cs_2AgBiBr_6$ Halide Double Perovskites. *J. Phys. Chem. C* **2022**, *126*, 10199−10208.
(19) Tailor, N. K.; Saini, S. K.; Yadav, P.; Kumar, M.; Satapathi, S. Elucidating Polaron Dynamics in $Cs_2AgBiBr_6$ Double Perovskite. *J. Phys. Chem. Lett.* **2023**, *14*, 730−736.
(20) Miyata, K.; Meggiolaro, D.; Trinh, M. T.; Joshi, P. P.; Mosconi, E.; Jones, S. C.; De Angelis, F.; Zhu, X.-Y. Large polarons in lead halide perovskites. *Sci. Adv.* **2017**, *3*, No. e1701217.
(21) Ambrosio, F.; Wiktor, J.; De Angelis, F.; Pasquarello, A. Origin of low electron−hole recombination rate in metal halide perovskites. *Energy Environ. Sci.* **2018**, *11*, 101−105.
(22) Wong, W. P.; Yin, J.; Chaudhary, B.; Chin, X. Y.; Cortecchia, D.; Lo, S.-Z. A.; Grimsdale, A. C.; Mohammed, O. F.; Lanzani, G.; Soci, C. Large polaron self-trapped states in three-dimensional metal-halide perovskites. *ACS Mater. Lett.* **2020**, *2*, 20−27.
(23) Jin, Z.; Peng, Y.; Fang, Y.; Ye, Z.; Fan, Z.; Liu, Z.; Bao, X.; Gao, H.; Ren, W.; Wu, J.; et al. Photoinduced large polaron transport and dynamics in organic−inorganic hybrid lead halide perovskite with terahertz probes. *Light Sci. Appl.* **2022**, *11*, 209.
(24) Lægsgaard, J.; Stokbro, K. Hole trapping at Al impurities in silica: A challenge for density functional theories. *Phys. Rev. Lett.* **2001**, *86*, 2834−2837.
(25) Lany, S.; Zunger, A. Polaronic hole localization and multiple hole binding of acceptors in oxide wide-gap semiconductors. *Phys. Rev. B* **2009**, *80*, 085202.
(26) Dabo, I.; Ferretti, A.; Poilvert, N.; Li, Y.; Marzari, N.; Cococcioni, M. Koopmans' condition for density-functional theory. *Phys. Rev. B* **2010**, *82*, 115121.
(27) Bischoff, T.; Wiktor, J.; Chen, W.; Pasquarello, A. Nonempirical hybrid functionals for band gaps of inorganic metal-halide perovskites. *Phys. Rev. Mater.* **2019**, *3*, 123802.
(28) Wiktor, J.; Pasquarello, A. Electron and hole polarons at the $BiVO_4$−water interface. *ACS Appl. Mater. Interfaces* **2019**, *11*, 18423−18426.
(29) Miceli, G.; Chen, W.; Reshetnyak, I.; Pasquarello, A. Nonempirical hybrid functionals for band gaps and polaronic distortions in solids. *Phys. Rev. B* **2018**, *97*, 121112.
(30) Wiktor, J.; Rothlisberger, U.; Pasquarello, A. Predictive determination of band gaps of inorganic halide perovskites. *J. Phys. Chem. Lett.* **2017**, *8*, 5507−5512.
(31) Zhao, X.-G.; Dalpian, G. M.; Wang, Z.; Zunger, A. Polymorphous nature of cubic halide perovskites. *Phys. Rev. B* **2020**, *101*, 155137.
(32) Cannelli, O.; Wiktor, J.; Colonna, N.; Leroy, L.; Puppin, M.; Bacellar, C.; Sadykov, I.; Krieg, F.; Smolentsev, G.; Kovalenko, M. V.; et al. Atomic-level description of thermal fluctuations in inorganic lead halide perovskites. *J. Phys. Chem. Lett.* **2022**, *13*, 3382−3391.
(33) Morana, M.; Wiktor, J.; Coduri, M.; Chiara, R.; Giacobbe, C.; Bright, E. L.; Ambrosio, F.; De Angelis, F.; Malavasi, L. Cubic or Not Cubic? Combined Experimental and Computational Investigation of the Short-Range Order of Tin Halide Perovskites. *J. Phys. Chem. Lett.* **2023**, *14*, 2178−2186.
(34) VandeVondele, J.; Krack, M.; Mohamed, F.; Parrinello, M.; Chassaing, T.; Hutter, J. Quickstep: Fast and accurate density functional calculations using a mixed Gaussian and plane waves approach. *Comput. Phys. Commun.* **2005**, *167*, 103−128.
(35) Kühne, T. D.; Iannuzzi, M.; Del Ben, M.; Rybkin, V. V.; Seewald, P.; Stein, F.; Laino, T.; Khaliullin, R. Z.; Schütt, O.;

https://doi.org/10.1021/acs.jpcc.3c06551
J. Phys. Chem. C 2023, 127, 23966−23972

Schiffmann, F.; et al. CP2K: An electronic structure and molecular dynamics software package-Quickstep: Efficient and accurate electronic structure calculations. *J. Chem. Phys.* **2020**, *152*, 194103.
(36) Kresse, G.; Hafner, J. Ab initio molecular dynamics for liquid metals. *Phys. Rev. B* **1993**, *47*, 558−561.
(37) Kresse, G.; Furthmüller, J. Efficient iterative schemes for ab initio total-energy calculations using a plane-wave basis set. *Phys. Rev. B* **1996**, *54*, 11169−11186.
(38) Goedecker, S.; Teter, M.; Hutter, J. Separable dual-space Gaussian pseudopotentials. *Phys. Rev. B* **1996**, *54*, 1703−1710.
(39) VandeVondele, J.; Hutter, J. Gaussian basis sets for accurate calculations on molecular systems in gas and condensed phases. *J. Chem. Phys.* **2007**, *127*, 114105.
(40) Perdew, J. P.; Ernzerhof, M.; Burke, K. Rationale for mixing exact exchange with density functional approximations. *J. Chem. Phys.* **1996**, *105*, 9982−9985.
(41) Guidon, M.; Hutter, J.; VandeVondele, J. Auxiliary density matrix methods for Hartree- Fock exchange calculations. *J. Chem. Theory Comput.* **2010**, *6*, 2348−2364.
(42) Blöchl, P. E. Projector augmented-wave method. *Phys. Rev. B* **1994**, *50*, 17953−17979.
(43) Freysoldt, C.; Neugebauer, J.; Van de Walle, C. G. Fully ab initio finite-size corrections for charged-defect supercell calculations. *Phys. Rev. Lett.* **2009**, *102*, 016402.
(44) Ziegler, T.; Rauk, A.; Baerends, E. J. On the calculation of multiplet energies by the Hartree-Fock-Slater method. *Theor. Chim. Acta* **1977**, *43*, 261−271.
(45) Sun, H.-Y.; Xiong, L.; Jiang, H. Toward first-principles approaches for mechanistic study of self-trapped exciton luminescence. *Chem. Phys. Rev.* **2023**, *4*, 031302.
(46) Daul, C. Density functional theory applied to the excited states of coordination compounds. *Int. J. Quantum Chem.* **1994**, *52*, 867−877.
(47) Falletta, S.; Wiktor, J.; Pasquarello, A. Finite-size corrections of defect energy levels involving ionic polarization. *Phys. Rev. B* **2020**, *102*, 041115.
(48) Steele, J. A.; Puech, P.; Keshavarz, M.; Yang, R.; Banerjee, S.; Debroye, E.; Kim, C. W.; Yuan, H.; Heo, N. H.; Vanacken, J.; et al. Giant electron−phonon coupling and deep conduction band resonance in metal halide double perovskite. *ACS Nano* **2018**, *12*, 8081−8090.
(49) Österbacka, N.; Erhart, P.; Falletta, S.; Pasquarello, A.; Wiktor, J. Small electron polarons in $CsPbBr_3$: Competition between electron localization and delocalization. *Chem. Mater.* **2020**, *32*, 8393−8400.
(50) Ouhbi, H.; Wiktor, J. Polaron formation and hopping in tantalate perovskite oxides: $NaTaO_3$ and $KTaO_3$. *Phys. Rev. B* **2021**, *104*, 235158.
(51) Momma, K.; Izumi, F. VESTA 3 for three-dimensional visualization of crystal, volumetric and morphology data. *J. Appl. Crystallogr.* **2011**, *44*, 1272−1276.
(52) Filip, M. R.; Hillman, S.; Haghighirad, A. A.; Snaith, H. J.; Giustino, F. Band gaps of the lead-free halide double perovskites $Cs_2BiAgCl_6$ and $Cs_2BiAgBr_6$ from theory and experiment. *J. Phys. Chem. Lett.* **2016**, *7*, 2579−2585.
(53) Palummo, M.; Berrios, E.; Varsano, D.; Giorgi, G. Optical properties of lead-free double perovskites by ab initio excited-state methods. *ACS Energy Lett.* **2020**, *5*, 457−463.
(54) Kentsch, R.; Scholz, M.; Horn, J.; Schlettwein, D.; Oum, K.; Lenzer, T. Exciton dynamics and electron−phonon coupling affect the photovoltaic performance of the $Cs_2AgBiBr_6$ double perovskite. *J. Phys. Chem. C* **2018**, *122*, 25940−25947.
(55) Zacharias, M.; Volonakis, G.; Giustino, F.; Even, J. Anharmonic electron-phonon coupling in ultrasoft and locally disordered perovskites. *npj Comput. Mater.* **2023**, *9*, 153.
(56) Even, J.; Pedesseau, L.; Jancu, J.-M.; Katan, C. Importance of spin−orbit coupling in hybrid organic/inorganic perovskites for photovoltaic applications. *J. Phys. Chem. Lett.* **2013**, *4*, 2999−3005.
(57) Ouhbi, H.; Ambrosio, F.; De Angelis, F.; Wiktor, J. Strong electron localization in tin halide perovskites. *J. Phys. Chem. Lett.* **2021**, *12*, 5339−5343.
(58) Berger, E.; Wiktor, J.; Pasquarello, A. Low-frequency dielectric response of tetragonal perovskite $CH_3NH_3PbI_3$. *J. Phys. Chem. Lett.* **2020**, *11*, 6279−6285.
(59) Ning, W.; Bao, J.; Puttisong, Y.; Moro, F.; Kobera, L.; Shimono, S.; Wang, L.; Ji, F.; Cuartero, M.; Kawaguchi, S.; et al. Magnetizing lead-free halide double perovskites. *Sci. Adv.* **2020**, *6*, No. eabb5381.
(60) Zelewski, S.; Urban, J.; Surrente, A.; Maude, D. K.; Kuc, A.; Schade, L.; Johnson, R.; Dollmann, M.; Nayak, P.; Snaith, H.; et al. Revealing the nature of photoluminescence emission in the metal-halide double perovskite $Cs_2AgBiBr_6$. *J. Mater. Chem. C* **2019**, *7*, 8350−8356.
(61) Wang, X.; Meng, W.; Liao, W.; Wang, J.; Xiong, R.-G.; Yan, Y. Atomistic mechanism of broadband emission in metal halide perovskites. *J. Phys. Chem. Lett.* **2019**, *10*, 501−506.
(62) Ismail-Beigi, S.; Louie, S. G. Self-trapped excitons in silicon dioxide: mechanism and properties. *Phys. Rev. Lett.* **2005**, *95*, 156401.
(63) Tal, A.; Liu, P.; Kresse, G.; Pasquarello, A. Accurate optical spectra through time-dependent density functional theory based on screening-dependent hybrid functionals. *Phys. Rev. Res.* **2020**, *2*, 032019.

https://doi.org/10.1021/acs.jpcc.3c06551
J. Phys. Chem. C 2023, 127, 23966−23972